



## Adsorption of linear and cyclic pentasiloxanes onto MCM-41: Experimental and computational studies

Camila M.A.C. Alves<sup>a,\*</sup>, Júlia F. Alves<sup>b</sup>, Lucas L. Bezerra<sup>c</sup>, Leonardo P. da Silva<sup>c</sup>, Norberto K.V. Monteiro<sup>c</sup>, Raimundo C. Rabelo-Neto<sup>d</sup>, Rinaldo S. Araújo<sup>b</sup>, Mona Lisa M. Oliveira<sup>a</sup>

<sup>a</sup> Universidade Estadual do Ceará, Campus do Itaperi, Centro de Ciências e Tecnologia, Fortaleza, Ceará, Brazil

<sup>b</sup> Instituto Federal do Ceará, Campus de Fortaleza, Departamento de Química e Meio Ambiente, Fortaleza, Ceará, Brazil

<sup>c</sup> Universidade Federal do Ceará, Campus do Pici, Departamento de Química Analítica e Físico-Química, Fortaleza, Ceará, Brazil

<sup>d</sup> Instituto Nacional de Tecnologia, Rio de Janeiro, Rio de Janeiro, Brazil

### ARTICLE INFO

**Keywords:**  
Siloxanes  
Adsorption  
MCM-41  
DFT simulations

### ABSTRACT

In this work MCM-41 solid was evaluated for the adsorption of dodecamethylpentasiloxane (L5) and decamethylcyclopentasiloxane (D5) siloxanes. The adsorbent was synthesized at room temperature using the sol-gel method and characterized by X-ray diffraction (XRD), scanning electron microscopy coupled to energy dispersive X-Ray spectroscopy (SEM-EDS), Fourier transform infrared spectroscopy (FTIR) and N<sub>2</sub> adsorption-desorption at 77 K. Adsorption equilibrium and kinetic studies were performed in isooctane at 25 °C in single and binary modes. The equilibrium data by Langmuir isotherm showed maximum adsorption capacity ( $q_{\max}$ ) of 0.058 mmol g<sup>-1</sup> (22.3 mg g<sup>-1</sup>) and 0.019 mmol g<sup>-1</sup> (7.05 mg g<sup>-1</sup>) for single mode of L5 and D5, respectively, while in binary mode these values were 0.054 (20.8 mg g<sup>-1</sup>) and 0.032 mmol g<sup>-1</sup> (11.9 mg g<sup>-1</sup>) for L5 and D5, respectively. The adsorption kinetics in both contact modes were typically of pseudo-first order. DFT simulations to calculate the adsorption energies between the ligands (siloxanes) and the receptor (MCM-41) showed a value of -0.76 eV for the MCM-L5 system, which is much higher than that found for MCM-D5 (-0.50 eV). This base research is important from an environmental and technological perspective, in which researchers will use the initial values obtained in this research to optimize the adsorbent matrix with an infinite number of modifications that can be made.

### 1. Introduction

Siloxanes are semi-volatile silicon compounds (VMS) that have a Si–O bond and an organic radical bonded to the silicon (Dankert, 2021). Due to specific physicochemical properties such as low flammability, low surface tension, and high thermal stability (Dankert, 2021; Katsoulis et al., 2017), siloxanes are used extensively for industrial purposes such as biopharmaceuticals, hygiene, and cosmetics products, among others (Kumari et al., 2023). Therefore, this high practicality makes these compounds found in detergents, shampoos, deodorants, and cosmetics be transported to environmental matrices (Xiang et al., 2021) and bio-fuels derived from landfills (de et al., 2015). VMS can be presented in two structural forms: linear (L) or cyclic (D) (Mojsiewicz-Pieńkowska and Krenczkowska, 2018). Decamethylcyclopentasiloxane (D5), for example, is the priority siloxane found in biogas, representing more than

90% of total siloxanes (Yang and Corsolini, 2019). Commonly, Octamethylcyclotetrasiloxane (D4), dodecamethylpentasiloxane (L5) and D5 are associated with damage to combustion engines that use biogas as fuel (Wang et al., 2020). Due to these harmful effects, several siloxanes removal methods are reported in literatures, with adsorption being one the most used techniques (Xiang et al., 2021; de Arespachoga et al., 2015). Adsorption is a mass transfer process that evaluates the capacity of materials to concentrate specific substances (in the liquid or gaseous phase) on their solid surface, thus enabling separation (Saleh and Saleh, 2022). It stands as one of the most effective methods in wastewater treatment, widely employed in industries to decrease the levels of environmentally toxic compounds in the effluents (Li et al., 2023).

Silicon-based mesoporous materials emerge as a choice for siloxane removal (Costa et al., 2020). They stand out for presenting a wide variety of applications in the most diverse environmental areas, with a

\* Corresponding author.

E-mail address: [camila.alves@aluno.uece.br](mailto:camila.alves@aluno.uece.br) (C.M.A.C. Alves).

<https://doi.org/10.1016/j.rsurfi.2024.100382>

Received 9 December 2024; Accepted 11 December 2024

Available online 12 December 2024

2666-8459/© 2024 The Authors. Published by Elsevier B.V. This is an open access article under the CC BY-NC-ND license (<http://creativecommons.org/licenses/by-nc-nd/4.0/>).

high surface area, great adsorption power, and good chemical and thermal stability due to the presence of silicon in the composition (Wang et al., 2022). Jiang et al. (2016) synthesized mesoporous aluminosilicate (UCT-15) varying aluminum dopant amounts and calcination heating rates for the adsorption removal of D4 from biogas. The best adsorption performance recorded was  $105 \text{ mg g}^{-1}$  at the Si/Al ratio = 5 and heating rate of  $10 \text{ }^\circ\text{C min}^{-1}$ , more than twice the adsorption amount compared to the commercial ZSM-5 (Jiang et al., 2016). In the other hand, Silva et al. (2021) investigated the use of silicon-based materials in the adsorption of siloxanes D4 and D5 in n-octane. The study revealed adsorption capacities of  $116 \text{ mg g}^{-1}$  for white silica gel,  $32 \text{ mg g}^{-1}$  for blue silica gel and  $72 \text{ mg g}^{-1}$  for synthesized silica derived from residual sand for D4 siloxane and 178, 59 and  $16 \text{ mg g}^{-1}$  for D5, respectively (Silva et al., 2021). Despite this, no one study was found in literatures that used the MCM-41 family of mesoporous materials for the adsorption of siloxanes.

Recent studies using computer simulations have been included to complement the experimental data obtained in adsorption systems (Wang et al., 2023). Floess and Murad (2011) reported the selective adsorption of siloxanes and water on amorphous silica (in simple and binary modes) and the temperature dependence of this competitive adsorption. The authors observed that the presence of water affects the adsorption of siloxane (PDMS) onto silica, while PDMS has an insignificant effect on water adsorption (Floess and Murad, 2011). It is known that the adsorption characteristics of siloxanes are strongly dependent on the surface structure of amorphous silica, however, there are few studies in literatures on estimates of adsorption energies between siloxanes and mesoporous materials.

In this context, the present work aims to investigate the adsorption equilibrium and kinetics in isooctane (liquid phase) of L5 and D5 in single and binary systems using MCM-41 as adsorbent. The experimental study will be corroborated through computational studies to verify the adsorption energy (DFT calculations) between the ligands studied (pentasiloxanes) and the mesoporous solid. This research is important from both an environmental perspective (reducing pollution in wastewater) and a technological standpoint (enhancing energy efficiency), particularly for industrial sectors relying on this biofuel as an energy source.

## 2. Experimental

### 2.1. Reagents

The model siloxanes molecules represented by dodecylmethylpentasiloxane (L5,  $384.8 \text{ g mol}^{-1}$ ) and decamethylcyclopentasiloxane (D5,  $370.8 \text{ g mol}^{-1}$ ) were provided by Sigma-Aldrich (Brazil). Tetraethyl orthosilicate (TEOS, Sigma-Aldrich, United States) and dodecylamine (Sigma-Aldrich, Brazil) were used as sources of silica and as a template for the synthesis of MCM-41, respectively. Aqueous  $\text{NH}_4\text{OH}$  by Isofar (Brazil) was employed in the alkaline condensation step and HCl (Sigma-Aldrich, Brazil) and ethanol 99.9% HPLC grade (Merck, Germany) were used to acidify the medium and serve as a solvent, respectively. Isooctane HPLC grade (Merck, Germany) was used to prepare organic of siloxanes solutions. He (carrier gas),  $\text{H}_2$  and  $\text{N}_2$  of 99.999% purity and synthetic air analytic grade (White Martins, Brazil) were used for analyzing the siloxanes by gas chromatography with flame ionization detector (GC-FID).

### 2.2. Synthesis of MCM-41

The synthesis of silicate mesoporous material (MCM-41) was carried out according to the sol-gel method adapted from Aguado et al. (2000) (Aguado et al., 2000) and Araújo et al. (2008) (Araújo et al., 2008). Initially, an acid hydrolysis step of silicon metal alkoxide (TEOS) in an ethanolic solution of dodecylamine was carried at  $\text{pH} = 2$  for 75 min under room temperature ( $25 \text{ }^\circ\text{C}$ ) and magnetic stirring. Subsequently,

the alkaline condensation step of the hydrolysis products was performed, involving the addition of an aqueous ammonia solution until  $\text{pH} = 10$ . The resulting product was allowed to aging in the ammoniacal liquor for 15 h to promote the formation of silanol groups on the mesoporous surface. Then, the precipitated solid was exhaustively washed and allowed to stand in a 1:1 mixture of ethanol/HCl 0.5 M for 24 h. Finally, the solid was washed with deionized water, filtered, and dried at  $105 \text{ }^\circ\text{C}$  in an oven for 12 h, followed by calcination in a muffle furnace with a ramp from 100 to  $550 \text{ }^\circ\text{C}$  at a rate of  $10 \text{ }^\circ\text{C min}^{-1}$  for approximately 3 h.

### 2.3. Characterization

The morphology of MCM-41 sample was determined using a scanning electron microscope (SEM) with a field emission electron gun (FEG-SEM) (ZEISS, Auriga 40) assisted by a Bruker E-Flash detector. Chemical composition analysis was conducted using the energy dispersive spectroscopy (EDS) module coupled to a microscope. The crystallographic analysis was performed using an X-ray diffractometer XRD-7000 (Shimadzu) with a  $\text{CuK}\alpha$  radiation source ( $\lambda = 1.5418 \text{ \AA}$ ). The diffractograms were recorded for low angle ( $2^\circ < 2\theta < 6^\circ$ ). The Fourier transform infrared spectra (FTIR) were collected on a Spectrum 100 FT-IR (PerkinElmer) in the region from  $450$  to  $4000 \text{ cm}^{-1}$  and with a spectral resolution of  $4 \text{ cm}^{-1}$ . The samples were prepared in the form of KBr pellets.  $\text{N}_2$  adsorption-desorption isotherms of the material were acquired at 77 K with an ASAP 2420 sorptometer (Micromeritics). Texture parameters such as Brunauer-Emmett-Teller specific surface area (BET), pore diameter and pore volume were determined using adsorption data in the relative pressure ( $p/p_0$ ) range of 0.05–0.30 from Barrett, Joyner and Halenda model (BJH).

### 2.4. Siloxane adsorption

The adsorption experiments were conducted following the methodology adapted from Silva et al. (2021) (Silva et al., 2021) to determine the adsorption capacities of the sample MCM-41 for adsorbates in single configuration (referred to as L5-Single and D5-Single) or as a binary mixture form (referred to as L5/D5-Binary) using isooctane as solvent. In all adsorptive tests, the concentrations of L5 and D5 siloxanes were determined according to the methodology of Cabrera-Codony et al., (2017) (Cabrera-Codony et al., 2017) using a GC-FID (TRACE™ GC 1310, Thermo Scientific) with a manual injection system (1 mL loop) and a capillary column of  $30 \text{ m} \times 0.53 \text{ mm} \times 3 \text{ }\mu\text{m}$  (BP-624, Capillary GC Column, SGE). The analytical runs were performed with a heating ramp of  $20^\circ \text{C min}^{-1}$  from  $80 \text{ }^\circ\text{C}$  to  $200 \text{ }^\circ\text{C}$ . The siloxane calibration curve was performed using external standards prepared from a stock solution of single and binary siloxanes solutions. The adsorption scheme was observed in Supplementary Material.

Thus, the equilibrium experiments were carried out using 50 mg of adsorbent in 20 mL of adsorbate solutions with concentrations ranging between 0.03 and  $1.1 \text{ mmol L}^{-1}$  for L5-Single, D5-Single and L5/D5-Binary ( $\sim 10$ – $400 \text{ mg L}^{-1}$ ). The tests were carried out in a Marconi® shaker MA 410 with a rotation of 150 rpm at a temperature of  $25 \text{ }^\circ\text{C}$  for 144 h, enough time for adsorption equilibrium to be reached. The adsorption capacity ( $q_e$ ) of siloxanes was calculated according to Equation (1):

$$q_e = \frac{(C_0 - C_e) V}{m} \quad (1)$$

Where:  $C_0$  and  $C_e$  are the initial and equilibrium concentrations of the adsorbates in solution ( $\text{mmol L}^{-1}$ ), respectively,  $V$  is the volume of siloxane solution (L) and  $m$  is the mass (g) of the adsorbent.

For all kinetic studies, 50 mg of the adsorbent was used in a 20 mL isooctane solution with a concentration of  $0.5 \text{ mmol L}^{-1}$  ( $\sim 200 \text{ mg L}^{-1}$ ) for L5-Single, D5-Single and L5/D5-Binary. Aliquots were taken at times

0, 4, 8, 24, 48, 72, 96, 120, and 144 h and quantified. The amount of adsorption  $q_t$  (mmol g<sup>-1</sup>) of adsorbates was calculated by mass balance, according to Eq. (1) previously described.

### 2.5. Equilibrium and kinetic modelling

Based on the adsorption equilibrium experiments, the isotherm parameters were calculated using the mathematical models of Langmuir, Temkin and Dubinin-Radushkevich, which were represented by Eqs. (2), (3) and (5), respectively. These isotherms are widely used in literatures to describe the batch adsorption equilibrium (Murphy et al., 2023).

$$q_e = \frac{q_{\max} K_L C_e}{1 + K_L C_e} \quad (2)$$

Where:  $q_e$  represents the adsorption capacity (mmol g<sup>-1</sup>) at equilibrium,  $C_e$  is the adsorbate concentration in the fluid phase (mmol L<sup>-1</sup>),  $q_{\max}$  is the maximum adsorption capacity (mmol g<sup>-1</sup>) and  $K_L$  is the Langmuir constant related to the enthalpy of adsorption (L mmol<sup>-1</sup>).

$$q_e = B \ln A_T C_e \quad (3)$$

$$B = \frac{RT}{b} \quad (4)$$

Where:  $A_T$  corresponds to the maximum binding energy constant (L g<sup>-1</sup>),  $B$  (J mol<sup>-1</sup>) is related to the heat of sorption,  $b$  is a Temkin isotherm constant,  $R$  is the universal ideal gas constant (8.314 J mol K<sup>-1</sup>) and  $T$  is the absolute temperature (K).

$$q_e = q_m e^{-\beta \varepsilon} \quad (5)$$

Where:  $q_m$  is Dubinin-Radushkevich monolayer capacity (mmol g<sup>-1</sup>),  $\beta$  is the constant related to the adsorption energy (mmol<sup>2</sup> J<sup>-2</sup>) and  $\varepsilon$  is the Polanyi potential.

The value of  $\varepsilon$  is calculated according to Eq. (6):

$$\varepsilon = RT \ln \left( 1 + \frac{1}{C_e} \right) \quad (6)$$

The constant  $\beta$  gives us the free energy of adsorption ( $E$ ) per adsorbate molecule, which can be calculated using the relationship expressed in Eq. (7).

$$E = \frac{1}{\sqrt{2\beta}} \quad (7)$$

The  $E$  value can be used to estimate the mechanism of the adsorption process (Bulut et al., 2008) (Bulut et al., 2008). When  $E < 8$  kJ mol<sup>-1</sup>, adsorption is controlled by physical forces, if  $E$  is in the range between 8 and 16 kJ mol<sup>-1</sup>, adsorption is associated with an ion exchange mechanism and finally if the value of  $E > 16$  kJ mol<sup>-1</sup>, adsorption can be attributed to diffusion into the particle (Özcan et al., 2006) (Özcan et al., 2006).

For mathematical modeling of adsorption kinetics, pseudo-first order, pseudo-second order and intraparticle diffusion models (Wang and Guo, 2022) (Wang and Guo, 2022) were applied, represented by Eqs. (8)–(10), respectively.

$$q_t = q_e (1 - e^{-k_1 t}) \quad (8)$$

Where:  $q_t$  (mmol g<sup>-1</sup>) is the amount adsorbed at time  $t$  (h),  $q_e$  represents the amount adsorbed at equilibrium (mmol g<sup>-1</sup>); and  $k_1$  is the pseudo first-order rate constant (h<sup>-1</sup>).

$$q_t = \frac{t}{\frac{1}{k_2 q_e} + \frac{1}{q_e}} \quad (9)$$

Where:  $k_2$  (g mmol<sup>-1</sup> h<sup>-1</sup>) is the pseudo second-order rate constant.

$$q_t = k_{int} t^{1/2} + C \quad (10)$$

Where:  $k_{int}$  (mmol g<sup>-1</sup> h<sup>-1/2</sup>) is the intraparticle diffusion rate constant, and  $C$  is a constant directly related to the boundary layer thickness.

### 2.6. Computational methodology

The tridimensional structure of each molecule is depicted in Fig. 1 and was drawn in the *Avogadro software* (Hanwell et al., 2012).

The computational calculations were carried out in stages. The first stage was the molecular dynamics of ligands L5 and D5 on the MCM-41 receptor. This step was carried out in the *xtb software* (Bannwarth et al., 2019) using 200 steps for each ligand/receptor system at a temperature of 298 K in the GFNO-xtb semiempirical force field. After these dynamics, the second step is carried out, which consists of optimizing each step of the dynamics in a more robust force field, the GFN2-xtb (Pracht et al., 2019), obtaining the energy of each optimized step of the system, and thus a ranking is made in terms of electronic energy, choosing the conformation with the lowest energy for the Density Functional Theory (DFT) step.

The MCM-L5 and MCM-D5 complexes were obtained in the *Molclus software* (Lu, 2016) and utilized as starting points for the quantum simulations. In sequence, the second part of the MCM-41 structure was removed from two complexes analyzed, followed by the addition of hydrogen atoms to complete the valence of the system (Fig. 2). All the single point energy calculations were performed based on the DFT through Cambridge Serial Total Energy Package (CASTEP) software (Clark et al., 2005). The Local Density Approximation (LDA) (Asahi et al., 1999) was parametrized with the CA-PZ functional as an exchange-correlation term (Ceperley and Alder, 1980). The cutoff energy employed in the simulations was 381.0 eV. Besides, the Brillouin-zone (BZ) k-Points sampling was obtained through Monkhorst-pack method with a 1 × 1 × 1 grid (Pack and Monkhorst, 1977).

Finally, the adsorption energy ( $E_{ads}$ ) calculations between the MCM-41 structure with the L5 and D5 molecules (adsorbate) by Eq. (11).

$$E_{ads} = E_{MCM-41/Adsorbate} - (E_{Adsorbate} + E_{MCM-41}) \quad (11)$$

Where:  $E_{MCM-41/Adsorbate}$ ,  $E_{Adsorbate}$ , and  $E_{MCM-41}$  terms are the total energies of the complex between the MCM-41 with the adsorbate, adsorbate in vacuum, and only the MCM-41 surface, respectively.

## 3. Results and discussion

### 3.1. Characterization

The synthesis procedure was conducted with a longer aging period (24 h) and without the reflux step, as compared to the original method (Araújo et al., 2008), which may have a direct impact on the chemical and textural properties of the solid. Fig. 3 shows some physical and chemical characteristics of the synthesized material.

Fig. 3a shows the XRD diffractogram of the synthesized sample. The low angle XRD analysis provides important information to understand the structural configuration of the synthesized material. The XRD pattern exhibits an intense peak at  $2\theta = 2.28^\circ$  corresponding to (100) diffraction peak, which is characteristic of MCM-41 materials with the mesoporous structure exhibiting an ordered hexagonal array (Dong et al., 2021). The absence of (110) and (200) diffraction peak in the range  $2\theta = 3.5$ – $4.5^\circ$  indicates the poor crystallinity of the synthesized material, as also observed by Aguado et al. (2008) (Aguado et al., 2000) and Mokaya (2001) (Mokaya, 2001). This behavior can be attributed to the lower temperature used in the preparation and the use of a short-chain surfactant ( $\leq C12$ ) (Mokaya, 2001; Khanmohammadi et al., 2021). The inset in Fig. 3a presents the EDS spectrum of MCM-41 and it reveals that the sample has  $47.9 \pm 5.26$  of silicon and  $52.1 \pm 1.62$  (%) of

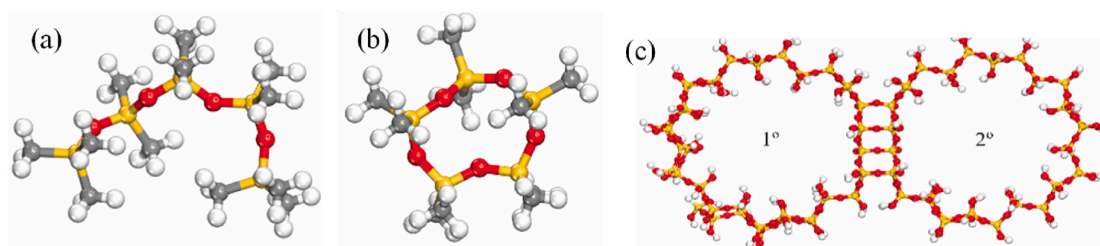


**Fig. 1.** Chemical structure of (a) dodecamethylpentasiloxane (L5), (b) decamethylcyclopentasiloxane (D5) and (c) MCM-41. Silicon atoms are shown in yellow, oxygen in red, carbon in gray and hydrogen in white.

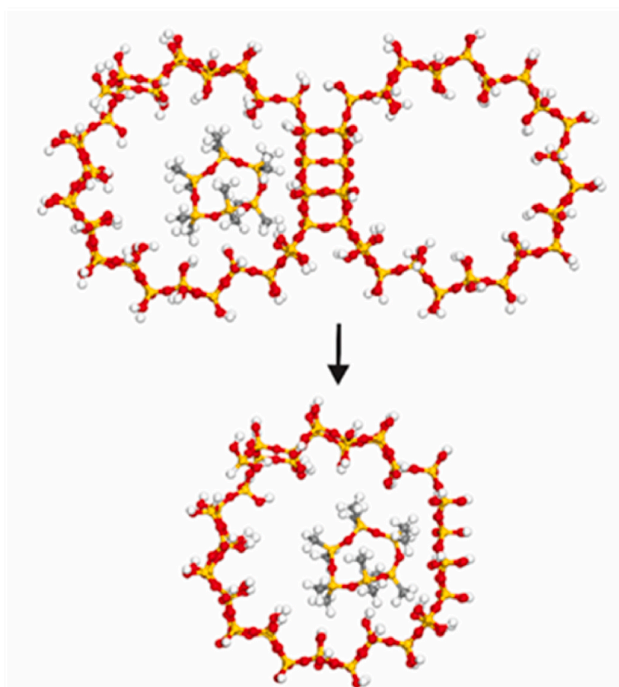


**Fig. 2.** Cutting the second part of the MCM-41 structure from all complexes simulated.

oxygen, which are very close to the values of pure silica.

In order to confirm the functional groups that make up the structure of the synthesized adsorbent, the FTIR spectrum of the sample is presented in Fig. 3b. The spectrum presents a broad band between 4000 and 3000  $\text{cm}^{-1}$ , which is related to the symmetrical and asymmetrical stretching vibrations of water bonds on the structural surface of MCM-41 (3400  $\text{cm}^{-1}$ ) (Heidari et al., 2009). Additionally, it can be simultaneously associated with O–H vibrations, originating from the Si–OH surface bonds of the silanol groups in different forms, either in its isolated form (3750  $\text{cm}^{-1}$ ), internal to the structure (3650  $\text{cm}^{-1}$ ) or hydrogen-bonded (3540  $\text{cm}^{-1}$ ) (Nguyen et al., 2018). This confirms the presence of silanol groups forming the mesoporous silica structure and indicates that it remained after the calcination. The band at 1630  $\text{cm}^{-1}$  can be attributed to O–H bending vibrations in the plane, associated with deformation of adsorbed water (Nguyen et al., 2018). Meanwhile, the broad band between 1000 and 1250  $\text{cm}^{-1}$  is related to stretching asymmetrical Si–O–Si. The appearance of the weak band at 970–962  $\text{cm}^{-1}$  may be related to the Si–O–Si stretching vibrations (Vaschetto et al., 2013).

The  $\text{N}_2$  adsorption-desorption isotherm of the material synthesized (Fig. 3c) exhibits a type IV isotherm with hysteresis at relative pressures

from 0.35 to 0.80, in accordance with the IUPAC classification (Sing et al., 1985). This observation suggests that the adsorption occurs in a monolayer, and the material possesses typical characteristics of mesoporous materials (Donohue and Aranovich, 1998). Based on the  $\text{N}_2$  adsorption-desorption isotherm, the synthesized sample exhibited the following structural and textural properties: a BET surface area of 694  $\text{m}^2 \text{g}^{-1}$ , mean pore diameter of 40.4 Å, and a volume pore size of 0.701  $\text{cm}^3 \text{g}^{-1}$ , which are consistent with the properties found by Araújo et al. (2008) for MCM-41 (Araújo et al., 2008) and can be compared with other studies in literatures (Sharma and Singh, 2022). Finally, the scanning electron microscopy (SEM) image of the material is presented in Fig. 3d, which reveal spherical, irregular, and slightly rough crystals, as also verified by Chen et al. (2019) (Chen et al., 2019).

### 3.2. Adsorption studies

The adsorption isotherms of L5-Single, D5-Single, and L5/D5-Binary at 25 °C in isooctane are presented in Fig. 4. Furthermore, the parameters obtained from the mathematical modeling of the isothermal models are shown in Table 1.

The  $q_{\text{max}}$  values found were 0.058  $\text{mmol g}^{-1}$  (22.3  $\text{mg g}^{-1}$ ), 0.019  $\text{mmol g}^{-1}$  (7.05  $\text{mg g}^{-1}$ ), 0.054  $\text{mmol g}^{-1}$  (20.8  $\text{mg g}^{-1}$ ) and 0.032  $\text{mmol g}^{-1}$  (11.9  $\text{mg g}^{-1}$ ) for L5-Single, D5-Single, L5-Binary and D5-Binary, respectively. In general, it is evident that the maximum adsorption capacity obtained from the Langmuir and Dubinin-Radushkevich mathematical models are similar to each other and close to the experimental value found (Table 1). The fit observed in the Langmuir Isotherm ( $R^2 > 0.90$ ) also indicates that adsorption occurred preferentially in a monolayer and that the surface is relatively homogeneous in terms of the distribution of active sites. The adsorption energy ( $E$ ) was less than 8  $\text{kJ mol}^{-1}$  in all scenarios, suggesting that the adsorption is governed by physical forces (Bulut et al., 2008; Özcan et al., 2006). The Temkin model demonstrated a good fit with values of  $B$  ( $\text{J mol}^{-1}$ ) directly proportional to  $q_{\text{max}}$  in both scenarios, indicating that the greater the adsorption capacity, the greater the heat of sorption (Soliman et al., 2019).

As depicted in Fig. 4, the results reveal two scenarios in the experiment. In the first scenario, there is a noticeable disparity in adsorption between L5 and D5 in their single mode, with MCM-41 showing L5-Single adsorption capacity around three times higher than that found for D5-Single (Fig. 4a). This difference in adsorption can be attributed to the structural dissimilarity between the two siloxanes. Despite both compounds having the same amount of silicon and similar molar mass, the cyclic structure of D5 is more stable and presents a greater structural complexity, typical of cyclic geometry. This stability in cyclic siloxanes is due to the greater number of O–Si–O bonds, which necessitates more energy to bend the oxygen atoms out of the tetrahedral configuration, protected by the loss of the methyl groups surrounding the cyclic structure (Wang et al., 2020).

Similar behavior was found in the gas phase study by Tran et al. (2019) using activated carbons as adsorbent at 20 °C  $\pm$  2 °C. The authors verified that the mass of adsorbed siloxane increases with the

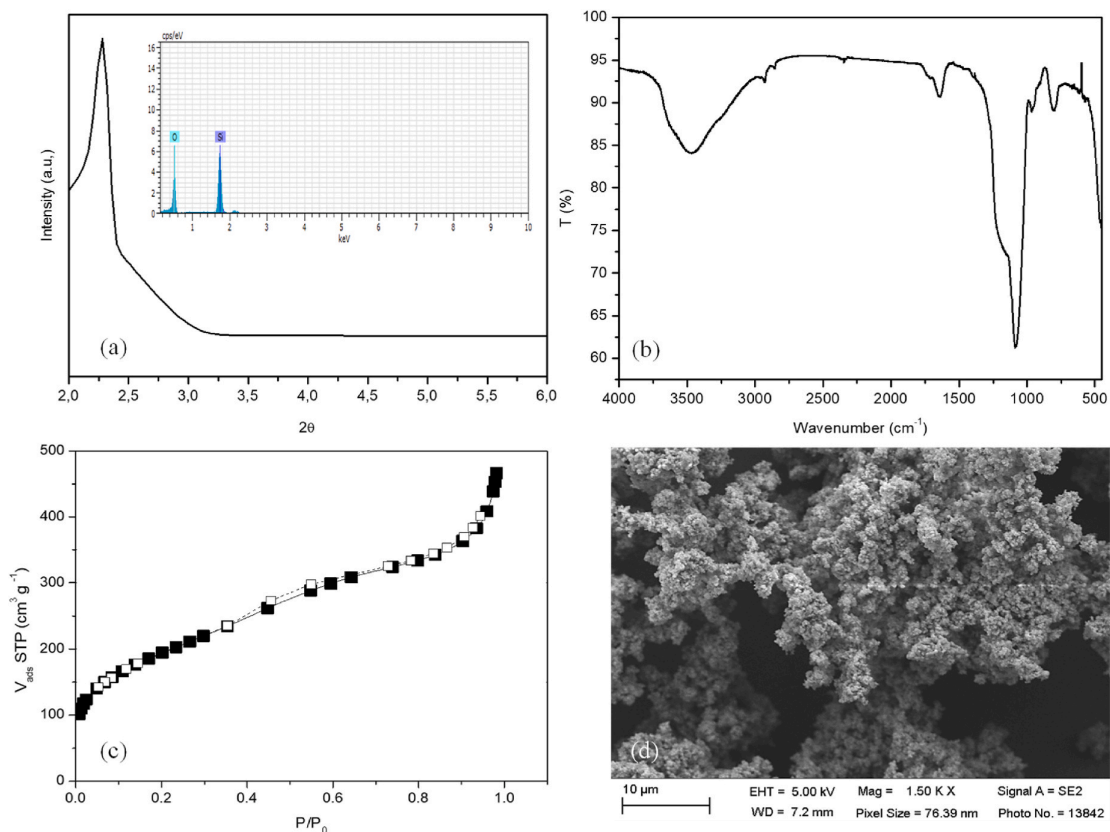


**Fig. 3.** Physicochemical, spectroscopic, textural properties and morphology of MCM-41 sample. (a) XRD diffractogram, (b) FTIR spectrum, (c) Nitrogen adsorption-desorption isotherm at 77 K and (d) SEM image.

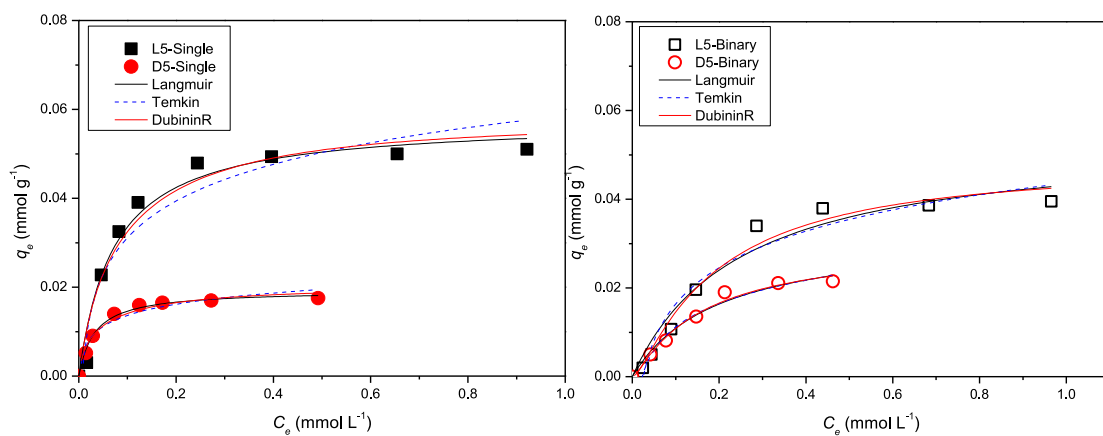


**Fig. 4.** Adsorption isotherms at 25 °C of L5 and D5 siloxanes onto MCM-41 in (a) single and (b) binary scenario.

**Table 1**

Equilibrium parameters at 25 °C for the adsorption of L5 and D5 onto MCM-41.

Adsorbate	Langmuir			Dubinin-Radushkevich			Temkin		
	$q_{max}$ (mmol g <sup>-1</sup> )	$K_L$ (L mmol <sup>-1</sup> )	$R^2$	$q_m$ (mmol g <sup>-1</sup> )	$E$ (kJ mol <sup>-1</sup> )	$R^2$	$A_T$ (L g <sup>-1</sup> )	$B$ (J mol <sup>-1</sup> )	$R^2$
L5-single	0.058	13.9	0.962	0.057	4.05	0.954	0.220	5.92	0.927
D5-single	0.019	27.2	0.992	0.021	4.65	0.976	1.17	1.35	0.956
L5-binary	0.054	4.03	0.959	0.047	3.78	0.978	0.104	4.56	0.977
D5-binary	0.032	5.05	0.977	0.028	4.08	0.983	0.118	2.81	0.978

increase of the chain length for the linear molecules while an opposite trend is found for cyclic ones (Tran et al., 2019). In the liquid phase, Silva et al. (2021) studied a D5 adsorption in n-octane at 20 °C using three different materials de silicon (>96% SiO<sub>2</sub>, 10–50 Å) as adsorbents in 168 h of contact. The maximum capacity was found to 178 mg g<sup>-1</sup> for white silica gel (795 m<sup>2</sup> g<sup>-1</sup>), 59 mg g<sup>-1</sup> for blue silica gel (472 m<sup>2</sup> g<sup>-1</sup>) and 16 mg g<sup>-1</sup> for synthesized silica from residual sand (512 m<sup>2</sup> g<sup>-1</sup>) (Silva et al., 2021).

In the binary scenario, there is weak competition between the siloxanes, which can be seen from the decrease in  $q_{\max}$  from L5-Single to L5-Binary and the increase in the value of  $q_{\max}$  in D5-Binary (Fig. 4b). However, the structural factor remains significant in the binary experiment, and the adsorption of L5-binary is about twice times higher than that found for D5-Binary (Table 1).

Cabrera-Codony et al., 2018 evaluated competitive adsorption in a multicomponent gas phase of limonene, toluene, and siloxanes (L2, D4 and D5) employing carbonaceous materials as adsorbents represented by microporous steam-derived activated carbons (SAC) and micro- and mesoporous phosphoric acid activated carbons (PhAC). The results revealed in the SAC groups an adsorption order of the type: limonene  $\gg$  D5 > D4 > L2  $\approx$  toluene, however, PhAC materials showed an inversion in this order with D5 being the most strongly adsorbed species (D5 > limonene > D4 > L2 > toluene). According to the authors, the acid character of these adsorbents, the presence of mesoporosity and their greater functionalization (groups containing O) promoted the greater adsorption capacity of cyclopentasiloxane (Cabrera-Codony et al., 2018). In contrast, in this work, despite the mesoporous nature of the MCM-41 sample, the low acidity typical of this material and the lower structural complexity of the linear molecule were decisive for the greater adsorption of L5 when compared to D5.

The experimental adsorption kinetics for the siloxanes L5-Single, D5-Single, L5-Binary, and D5-Binary at 25 °C onto MCM-41 are shown in Fig. 5. The numerical parameters obtained from kinetic modeling are summarized in Table 2.

In Fig. 5a, the non-linear plots in all scenarios suggest that the adsorption process of single and binary siloxanes follow the pseudo-first order kinetics when considering the high correlation coefficients found ( $R^2$  between 0.978 and 0.996) and the similarity between the  $q_e$  (experimental) and  $q_t$  (calculated) (Table 2). On the other hand, for the pseudo-second order model, despite the high values of the correlation coefficient ( $R^2 > 0.931$ ), the values of  $q_t$  are very different from those found experimentally ( $q_e$ ). In addition, the equilibrium is reached more rapidly for D5 than L5 in both experiments, with single and binary systems with a 72 h for D5 and 96 h for L5, approximately. This relatively slow kinetics has been reported in literatures for D4 in the liquid phase by Popat and Deshusses (2008) (Popat and Deshusses, 2008) and

for both D4 and D5 in the liquid phase by Silva et al. (2021) (Silva et al., 2021).

Fig. 5b shows the linear graph of  $q_t$  versus  $t^{1/2}$  for the intraparticle diffusion model of the L5-Single, D5-Single and L5/D5-Binary adsorption on the MCM-41. The linear slope represents the internal diffusion parameter and the point on the line that intersects the y-axis provides information on the thickness of the boundary layer (Wang and Guo, 2022). The data from the present study show a multilinearity, indicating that two or more steps occur during the adsorptive process (Bulut et al., 2008; Özcan et al., 2006). In this case, the first step (adsorption on the external surface), which is considered the fastest, is absent, and only starts from the intraparticle diffusion step (adsorption rate-limiting step) lasting from 4 to 81 h. Finally, the experiment reaches the last step, which is related to the final equilibrium, where intraparticle diffusion starts to slow down due to lower concentrations of the adsorbate in the solution (100–144 h). A similar result was observed by Yang et al. (2022) when they used activated carbon containing CuO for the adsorption of siloxane D4 in the gas phase (Yang et al., 2022). The results of the intraparticle diffusion models also indicated that adsorption occurs in two distinct main steps, corresponding to the intraparticle diffusion and adsorption equilibrium stage.

### 3.3. Computational results

The energies  $E_{(MCM-41/Adsorbate)}$  obtained from the interaction calculations indicate that ligand L5 is more favored to interact with the MCM-41 receptor, obtaining a value of -0.76 eV (Fig. 6). Thus, there is a difference of 0.26 eV for the interaction between D5 and MCM-41 (-0.50 eV).

This behavior may be related to the larger contact area of the L5 ligand, which has an open chain shape, compared to the cyclic ligands. The results indicate that the tendency to favor the adsorption of D5 is inversely proportional to the size of the cyclic structure of the ligand, corroborating with the experimental results. A work by Yang et al., (2022) in gas phase introduced copper oxides (CuO) into activated carbon (AC) by impregnation to improve the adsorption performance of D4. As in the present work, the adsorption combined experimental studies and theoretical calculations. The adsorption experiments demonstrated that CuO introduction could significantly improve the adsorption performance, where the 10-CuO/AC-800 material obtained the best adsorption performance (1.67 mmol g<sup>-1</sup>). DFT calculations indicated that the adsorption energy of the siloxane D4 molecule on the CuO surface is approximately -1.40 eV, which is higher than other adsorption sites (Yang et al., 2022). In other words, modifications to the adsorbent matrix to add an acidic or alkaline character may be an alternative to increase adsorption capacities and energies. Thus, the

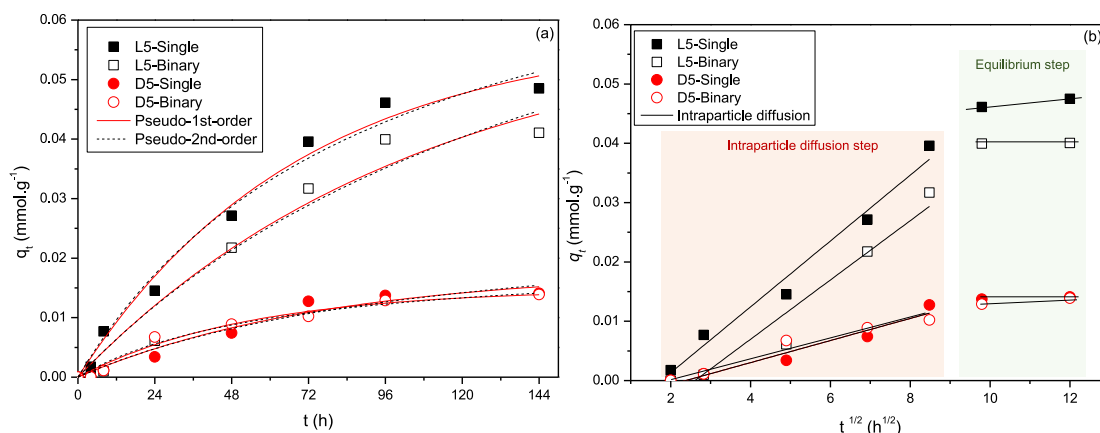
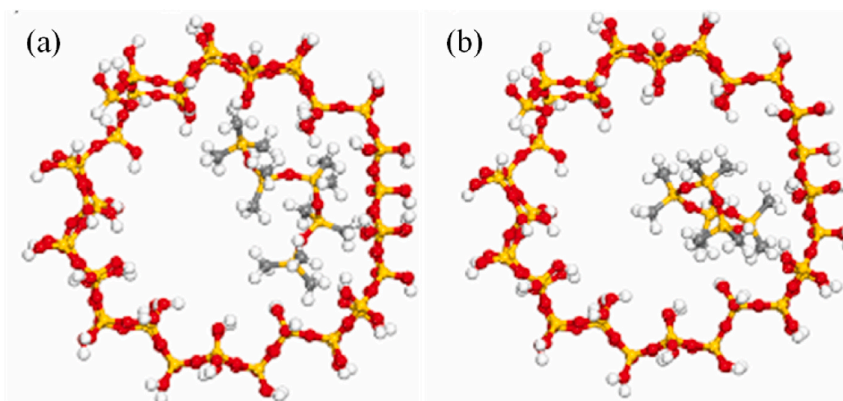


Fig. 5. Adsorption kinetics at 25 °C of L5 and D5 siloxanes onto MCM-41 in (a) pseudo first- and second-orders models and (b) intraparticle diffusion model.

**Table 2**  
Kinetics parameters at 25 °C for the adsorption of L5 and D5 onto MCM-41.

Adsorbate ( $C_0 = 0.50 \text{ mmol L}^{-1}$ )		Pseudo-first order			Pseudo-second order			Intraparticle diffusion	
System	$q_{e,exp}$ ( $\text{mmol g}^{-1}$ )	$q_t$ ( $\text{mmol g}^{-1}$ )	$k_1$ ( $\text{h}^{-1}$ )	$R^2$	$q_t$ ( $\text{mmol g}^{-1}$ )	$k_2$ ( $\text{g mmol}^{-1} \text{ h}^{-1}$ )	$R^2$	$k_{int}$ ( $\text{mmol g}^{-1} \text{ h}^{1/2}$ )	$R^2$
L5-single	0.049	0.058	0.015	0.996	0.085	0.126	0.983	0.0051	0.961
D5-single	0.018	0.018	0.012	0.980	0.028	0.108	0.953	0.0014	0.931
L5-binary	0.038	0.046	0.015	0.978	0.069	0.115	0.972	0.0038	0.950
D5-binary	0.021	0.025	0.011	0.986	0.020	0.040	0.983	0.0020	0.963



**Fig. 6.** Adsorption energies of the (a) MCM-L5 and (b) MCM-D5 complexes.

original and initial work using MCM-41 will serve as a basis for researchers to seek better conditions through this material functionalization for siloxanes removal.

#### 4. Conclusions

The synthesized material presented chemical and textural properties consistent with other materials in the MCM-41 family reported in literature. In studies of equilibrium and adsorption kinetics in liquid phase (isooctane) at room temperature was observed that D5 had a lower adsorption capacity ( $0.019 \text{ mmol g}^{-1}$  and  $0.032 \text{ mmol g}^{-1}$  for D5-Single and D5-Binary, respectively) compared to L5 ( $0.058 \text{ mmol g}^{-1}$  and  $0.054 \text{ mmol g}^{-1}$  for L5-Single and L5-Binary configurations), mainly due to the structural difference between the two compounds. This was confirmed from computational calculations that predicted that the adsorption energy between L5 and MCM-41 was greater ( $-0.76 \text{ eV}$ ) than the energy of the MCM-D5 complex ( $-0.50 \text{ eV}$ ). The mesoporous solid MCM-41, despite not being recognized as the best adsorbent, had not yet been studied in its pure form in the MCM-41/L5-D5 system. In other words, the use of MCM-41 as the only adsorbent in the present research was intentional since the experimental and computational studies of the pure matrix will be used as a reference for other MCM-41 functionalizations (Al addition, for example), in order to increase the adsorption capacity of siloxanes in future work, and better understand the interaction of liquid or gas siloxanes with different adsorbents.

#### CRediT authorship contribution statement

**Camila M.A.C. Alves:** Conceptualization, Formal analysis, Methodology, Writing – original draft. **Júlia F. Alves:** Formal analysis, Methodology. **Lucas L. Bezerra:** Data curation, Methodology, Software. **Leonardo P. da Silva:** Data curation, Methodology, Software. **Norberto K.V. Monteiro:** Data curation, Formal analysis, Methodology, Software. **Raimundo C. Rabelo-Neto:** Data curation, Methodology, Validation. **Rinaldo S. Araújo:** Conceptualization, Methodology, Writing – review & editing. **Mona Lisa M. Oliveira:** Conceptualization, Supervision,

Writing – review & editing.

#### Declaration of competing interest

The authors declare that they have no known competing financial interests or personal relationships that could have appeared to influence the work reported in this paper.

#### Acknowledgment

This research was supported by the Brazilian agency CAPES (Coordenação de Aperfeiçoamento de Pessoal de Nível Superior). This work was also supported by FUNCAP (Fundação Cearense de Apoio ao Desenvolvimento Científico e Tecnológico) through the FUNCAP/CEGAS Project [No. 8912401/2018].

#### Appendix A. Supplementary data

Supplementary data to this article can be found online at <https://doi.org/10.1016/j.rsurfi.2024.100382>.

#### Data availability

No data was used for the research described in the article.

#### References

- Aguado, J., Serrano, D.P., Escola, J.M., 2000. A sol-gel approach for the room temperature synthesis of Al-containing micelle-templated silica. *Microporous Mesoporous Mater.* 34, 43–54. [https://doi.org/10.1016/S1387-1811\(99\)00154-7](https://doi.org/10.1016/S1387-1811(99)00154-7).
- Araújo, R.S., Azevedo, D.C.S., Cavalcante Jr., C.L., Jiménez-López, A., Rodríguez-Castellón, E., 2008. Adsorption of polycyclic aromatic hydrocarbons (PAHs) from isooctane solutions by mesoporous molecular sieves: influence of the surface acidity. *Microporous Mesoporous Mater.* 108, 213–222. <https://doi.org/10.1016/j.micromeso.2007.04.005>.
- Asahi, R., Mannstadt, W., Freeman, A.J., 1999. Optical properties and electronic structures of semiconductors with screened-exchange LDA. *Phys. Rev. B* 59, 7486. <https://doi.org/10.1103/PhysRevB.59.7486>.
- Bannwarth, C., Ehlert, S., Grimme, S., 2019. GFN2-xTB – an accurate and broadly parametrized self-consistent tight-binding quantum chemical method with multipole

- electrostatics and density-dependent dispersion contributions. *J. Chem. Theor. Comput.* 15, 1652–1671. <https://doi.org/10.1021/acs.jctc.8b01176>.
- Bulut, E., Özacar, M., Şengil, I.A., 2008. Adsorption of malachite green onto bentonite: equilibrium and kinetic studies and process design. *Microporous Mesoporous Mater.* 115 (3), 234–246. <https://doi.org/10.1016/j.micromeso.2008.01.039>.
- Cabrera-Codony, A., Georgi, A., Gonzalez-Olmos, R., Valdés, H., Martín, M.J., 2017. Zeolites as recyclable adsorbents/catalysts for biogas upgrading: removal of octamethylcyclotetrasiloxane. *J. Chem. Eng.* 307, 820–827. <https://doi.org/10.1016/j.ccej.2016.09.017>.
- Cabrera-Codony, A., Santos-Clotas, E., Ania, C.O., Martín, M.J., 2018. Competitive siloxane adsorption in multicomponent gas streams for biogas upgrading. *J. Chem. Eng.* 344, 565–573. <https://doi.org/10.1016/j.ccej.2018.03.131>.
- Ceperley, D.M., Alder, B.J., 1980. Ground state of the electron gas by a stochastic method. *Phys. Rev. Lett.* 45, 566. <https://doi.org/10.1103/PhysRevLett.45.566>.
- Chen, D., Yang, Y., Zhang, X., Wang, X., Xu, Y., Qian, G., 2019. Mesoporous composite NiCr<sub>2</sub>O<sub>4</sub>/Al-MCM-41: a novel photocatalyst for enhanced hydrogen production. *Int. J. Hydrogen Energy* 44 (33), 18123–18133. <https://doi.org/10.1016/j.ijhydene.2019.03.106>.
- Clark, S.J., Segall, M.D., Pickard, C.J., Hasnip, P.J., Probert, M.I.J., Refson, K., Payne, M. K., 2005. First principles methods using CASTEP. *Z. für Kristallogr. - Cryst. Mater.* 220, 567–570. <https://doi.org/10.1524/zkri.220.5.567.65075>.
- Costa, J.A.S., de Jesus, R.A., Santos, D.O., Mano, J.F., Romão, L.P.C., Paranhos, C.M., 2020. Recent progresses in the adsorption of organic, inorganic, and gas compounds by MCM-41-based mesoporous materials. *Microporous Mesoporous Mater.* 291, 109698. <https://doi.org/10.1016/j.micromeso.2019.109698>.
- Dankert, C., 2021. von Hänisch, Siloxane Coordination Revisited: Si–O Bond character, reactivity and magnetic molecular shapes. *Eur. J. Inorg. Chem.* 2021, 2907–2927. <https://doi.org/10.1002/ejic.202100275>.
- de Arespacochaga, N., Valderrama, C., Raich-Montiu, J., Crest, M., Mehta, S., Cortina, J. T., 2015. Understanding the effects of the origin, occurrence, monitoring, control, fate and removal of siloxanes on the energetic valorization of sewage biogas – a review. *Renew. Sustain. Energy Rev.* 52, 366–381. <https://doi.org/10.1016/j.rser.2015.07.106>.
- Dong, C., Deng, X., Guo, X., Wang, B., Ye, X., Fan, J., Zhu, C., Fan, F., Qing, B., 2021. Synthesis of potassium metal ferrocyanide/Al-MCM-41 with fast and selective adsorption of cesium. *Colloids Surf., A: Physicochem. Eng.* 613, 126107. <https://doi.org/10.1016/j.colsurfa.2020.126107>.
- Donohue, M.D., Aranovich, G.L., 1998. Classification of Gibbs adsorption isotherms. *Adv. Colloid Interface Sci.* 76–77, 137–152. [https://doi.org/10.1016/S0001-8686\(98\)00044-X](https://doi.org/10.1016/S0001-8686(98)00044-X).
- Floess, J.K., Murad, S., 2011. Molecular simulations of the competitive adsorption of siloxanes and water on amorphous silica surfaces as a function of temperature. *Chem. Phys. Lett.* 516 (4–6), 216–219. <https://doi.org/10.1016/j.cplett.2011.09.085>.
- Hanwell, M.D., Curtis, D.E., Lonie, D.C., Vandermeersch, T., Zurek, E., Hutchison, G.R., 2012. Avogadro: an advanced semantic chemical editor, visualization, and analysis platform. *J. Cheminf.* 4, 1–17. <https://doi.org/10.1186/1758-2946-4-17>.
- Heidari, A., Younesi, H., Mehraban, Z., 2009. Removal of Ni (II), Cd (II), and Pb (II) from a ternary aqueous solution by amino functionalized mesoporous and nano mesoporous silica. *J. Chem. Eng.* 153 (1–3), 70–79. <https://doi.org/10.1016/j.ccej.2009.06.016>.
- Jiang, T., Zhong, W., Jafari, T., Du, S., He, J., Fu, Y., Singh, P., Suib, S.L., 2016. Siloxane D4 adsorption by mesoporous aluminosilicates. *Chem. Eng. J.* 289, 356–364. <https://doi.org/10.1016/j.ccej.2015.12.094>.
- Katsoulis, D.E., Schmidt, R.G., Zank, G.A., 2017. Chapter 7 – siloxanes and silicones. In: Lee, Vladimir Ya (Ed.), *Advances in Silicone Technologies 2000–15*, Organosilicon Compounds. Academic Press, pp. 301–322. <https://doi.org/10.1016/B978-0-12-814213-4.00007-1>.
- Khanmohammadi, M., Shahrouzi, J.R., Rahmani, F., 2021. Insights into mesoporous MCM-41-supported titania decorated with CuO nanoparticles for enhanced photodegradation of tetracycline antibiotic. *Environ. Sci. Pollut. Res.* 28, 862–879. <https://doi.org/10.1007/s11356-020-10546-0>.
- Kumari, K., Singh, A., Marathe, D., 2023. Cyclic volatile methyl siloxanes (D4, D5, and D6) as the emerging pollutants in environment: environmental distribution, fate, and toxicological assessments. *Environ. Sci. Pollut. Res.* <https://doi.org/10.1007/s11356-023-25568-7> (in press).
- Li, S., Wang, D., Qiu, Y., Wang, L., Yang, L., 2023. Application of macrocycle-crosslinked polymers as adsorbents for the removal of organic micropollutants from water. *Curr. Opin. Green Sustainable Chem.* 40, 100755. <https://doi.org/10.1016/j.cogsc.2023.100755>.
- Lu, T., 2016. Molclus program, version 1.12. In: Beijing Kein Research Center for Natural Science, China. <http://www.keinsci.com/research/molclus.html>. (Accessed 1 October 2023).
- Mojsiewicz-Pieńkowska, K., Krenczkowska, D., 2018. Evolution of consciousness of exposure to siloxanes – review of publications. *Chemosphere* 191, 204–217. <https://doi.org/10.1016/j.chemosphere.2017.10.045>.
- Mokaya, R., 2001. Observation of some pore wall ordering in mesoporous silica. *Chem. Commun.* 12, 1092–1093. <https://doi.org/10.1039/B1018120>.
- Murphy, O.P., Vashishtha, M., Palanisamy, P., Kumar, K.V., 2023. A Review on the adsorption isotherms and design calculations for the optimization of adsorbent mass and contact time. *ACS Omega* 8 (20), 17407–17430. <https://doi.org/10.1021/acsomega.2c08155>.
- Nguyen, T.T., Le, G.H., Le, C.H., Nguyen, M.B., Quan, T.T., Pham, T.T., Vu, T.A., 2018. Atomic implantation synthesis of Fe-Cu/SBA-15 nanocomposite as a heterogeneous Fenton-like catalyst for enhanced degradation of DDT. *Mater. Res. Express* 5 (11), 115005. <https://doi.org/10.1088/2053-1591/aadce1>.
- Özcan, A., Öncü, E.M., Özcan, A.S., 2006. Kinetics, isotherm and thermodynamic studies of adsorption of Acid Blue 193 from aqueous solutions onto natural sepiolite. *Colloids Surf., A: Physicochem. Eng.* 277 (1–3), 90–97. <https://doi.org/10.1016/j.colsurfa.2005.11.017>.
- Pack, J.D., Monkhorst, H.J., 1977. Special points for Brillouin-zone integrations – a reply. *Phys. Rev. B* 16, 1748. <https://doi.org/10.1103/PhysRevB.16.1748>.
- Popat, S.C., Deshusses, M.A., 2008. Biological removal of siloxanes from landfill and digester gases: opportunities and challenges. *Environ. Sci. Technol.* 42, 8510–8515. <https://doi.org/10.1021/es801320w>.
- Pracht, P., Caldeweyher, E., Ehlert, S., Grimme, S., 2019. A Robust non-self-consistent tight-binding quantum chemistry method for large molecules. *Chem* 1–19. <https://doi.org/10.26434/chemrxiv.8326202.v1>.
- Saleh, T.A., 2022. Chapter 2 – adsorption technology and surface science. In: Saleh, Tawfik A. (Ed.), *Interface Sci. Technol.*, vol. 34. Elsevier, pp. 39–64. <https://doi.org/10.1016/B978-0-12-849876-7.00006-3>.
- Sharma, S., Singh, U.P., 2022. MCM-41 supported heterogeneous catalyst for the conversion of alkene to epoxide: synthesis, characterization and catalytic studies. *Inorg. Chem. Commun.* 139, 109359. <https://doi.org/10.1016/j.inoche.2022.109359>.
- Silva, E.N., Cantillo-Castrillon, M., Dantas, T.M., Mesquita, Y.M., Maia, D.A.S., Bastos-Neto, M., Barcellos, W.M., Azevedo, D.C.S., 2021. Siloxane adsorption by porous silica synthesized from residual sand of wastewater treatment. *J. Environ. Chem. Eng.* 9 (2), 104805. <https://doi.org/10.1016/j.jece.2020.104805>.
- Sing, K.S.W., Everett, D.H., Haul, R.A.W., Moscou, L., Pierotti, R.A., Rouquérol, J., Siemieniowska, T., 1985. Reporting physisorption data for gas/solid systems with special reference to the determination of surface area and porosity. *Pure Appl. Chem.* 57 (4), 603–619. <https://doi.org/10.1351/pac198557040603>.
- Soliman, M.A., Rashad, G.M., Mahmoud, M.R., 2019. Development of the adsorption capability of MCM-41 particles synthesized at room temperature using 8-hydroxyquinoline-5-sulfonic acid for removal of Co(II) and Cr(VI) in binary systems. *Chem. Eng. Res. Des.* 144, 459–471. <https://doi.org/10.1016/j.cherd.2019.02.032>.
- Tran, V.T.L., Gélín, P., Ferronato, C., Chovelon, J., Fine, L., Postole, G., 2019. Adsorption of linear and cyclic siloxanes on activated carbons for biogas purification: sorbents regenerability. *J. Chem. Eng.* 378, 122152. <https://doi.org/10.1016/j.ccej.2019.122152>.
- Vaschetto, E.G., Monti, G.A., Herrero, E.R., Casuscelli, S.G., Eimer, G.A., 2013. Influence of the synthesis conditions on the physicochemical properties and acidity of Al-MCM-41 as catalysts for the cyclohexanone oxime rearrangement. *Appl. Catal., A* 453, 391–402. <https://doi.org/10.1016/j.apcata.2012.12.016>.
- Wang, J., Guo, X., 2022. Rethinking of the intraparticle diffusion adsorption kinetics model: interpretation, solving methods and applications. *Chemosphere* 309 (2), 136732. <https://doi.org/10.1016/j.chemosphere.2022.136732>.
- Wang, N., Tan, L., Xie, L., Wang, Y., Ellis, T., 2020. Investigation of volatile methyl siloxanes in biogas and the ambient environment in a landfill. *J. Environ. Sci.* 91, 54–61. <https://doi.org/10.1016/j.jes.2020.01.005>.
- Wang, D., Chen, X., Feng, J., Sun, M., 2022. Recent advances of ordered mesoporous silica materials for solid-phase extraction. *J. Chromatogr., A* 1675, 463157. <https://doi.org/10.1016/j.chroma.2022.463157>.
- Wang, J., Liu, L., Wang, L., Lu, J., Li, Y., 2023. Volatile methyl siloxane separation from biogas using hollow fiber membrane contactor with polyethylene glycol dimethyl ether: a numerical and experimental study. *Process Saf. Environ. Protect.* 171, 250–259. <https://doi.org/10.1016/j.psep.2023.01.023>.
- Xiang, X., Liu, N., Xu, L., Cai, Y., 2021. Review of recent findings on occurrence and fates of siloxanes in environmental compartments. *Ecotoxicol. Environ. Saf.* 224, 112631. <https://doi.org/10.1016/j.ecoenv.2021.112631>.
- Yang, L., Corsolini, S.I., 2019. Online removal of volatile siloxanes in solid-state anaerobic digester biogas using a biofilter and an activated carbon filter. *J. Environ. Chem. Eng.* 7 (5), 103284. <https://doi.org/10.1016/j.jece.2019.103284>.
- Yang, Z., Chen, Z., Gong, H., Wang, X., 2022. Copper oxide modified activated carbon for enhanced adsorption performance of siloxane: an experimental and DFT study. *Appl. Surf. Sci.* 601, 154200. <https://doi.org/10.1016/j.apsusc.2022.154200>.